nature geoscience

LETTERS

PUBLISHED ONLINE: 7 DECEMBER 2015 | DOI: 10.1038/NGEO2603

Deglacial Indian monsoon failure and North Atlantic stadials linked by Indian Ocean surface cooling

Jessica E. Tierney[1,2]*, Francesco S. R. Pausata[3] and Peter deMenocal[4]

The Indian monsoon, the largest monsoon system on Earth, responds to remote climatic forcings, including temperature changes in the North Atlantic[1,2]. The monsoon was weak during two cool periods that punctuated the last deglaciation—Heinrich Stadial 1 and the Younger Dryas. It has been suggested that sea surface cooling in the Indian Ocean was the critical link between these North Atlantic stadials and monsoon failure[3]; however, based on existing proxy records[4] it is unclear whether surface temperatures in the Indian Ocean and Arabian Sea dropped during these intervals. Here we compile new and existing temperature proxy data[4–7] from the Arabian Sea, and find that surface temperatures cooled whereas subsurface temperatures warmed during both Heinrich Stadial 1 and the Younger Dryas. Our analysis of model simulations shows that surface cooling weakens the monsoon winds and leads to destratification of the water column and substantial subsurface warming. We thus conclude that sea surface temperatures in the Indian Ocean are indeed the link between North Atlantic climate and the strength of the Indian monsoon.

During the transition from the Last Glacial Maximum (LGM) to the Holocene (about 20,000–10,000 yr BP), two abrupt, millennial-scale coolings interrupted a gradually warming climate: Heinrich Stadial 1 (H1; 17,500–14,500 yr BP) and the Younger Dryas (YD; 12,800–11,500 yr BP). These events are associated with the sudden release of freshwater into the North Atlantic, which slowed thermohaline circulation[8], cooled the Northern Hemisphere, and had far-reaching effects on global climate[9,10]. In the tropics, the Indian monsoon system weakened, causing dry conditions throughout the Indian Ocean rim[11]. Although these events are specific to a glaciated climate state, they highlight the teleconnection between the North Atlantic and the tropical monsoons. Understanding how warmings and coolings in the North Atlantic impact the world's largest monsoon system may improve our ability to predict future changes in the Indian monsoon domain.

Previous modelling work suggests that sea surface temperatures (SSTs) in the Indian Ocean are the crucial link between North Atlantic cooling and monsoon failure during Heinrich Events[3]. Specifically, cooling in the Indian Ocean, which is most pronounced in the western part of the basin, causes a delayed onset of the monsoon and weakened convection[3]. If SSTs do not cool, the Indian monsoon is largely unaffected in these simulations, even though the cooling in the Northern Hemisphere causes a southward shift in the tropical convergence zones[3]. This implicates cool Indian Ocean SSTs—and not just a change in the hemispheric temperature gradients—as a necessary precursor for a weakening of the Indian monsoon during these millennial-scale events. However, some proxy data suggest that the Arabian Sea—where the model shows a strong decrease in temerature—may not have cooled during H1 (ref. 4), questioning whether this proposed mechanism for monsoon failure is valid.

Here, we analyse temperature proxy evidence from the Arabian Sea during the deglaciation to explicitly test the hypothesis that the surface ocean cooled during H1 and the YD. We then compare the proxy data to both timeslice and transient climate simulations to understand more generally the regional oceanic response to these millennial-scale events. The temperature proxy data include Mg/Ca and $\delta^{18}O$ measured on the planktonic foraminifera *Globigerinoides ruber* (white), and the lipid-based alkenone ($U^{K'}_{37}$), and glycerol dialkyl glycerol tetraether (GDGT) (TEX_{86}) indices. We use published, publicly available proxy time series that have adequate chronology and time resolution to resolve H1 and the YD, and also present new proxy data from core P178-15P in the Gulf of Aden, which has a well-defined chronology[12,13]. In addition, we include data from a timeslice study[5] that provide a spatial array of paired Mg/Ca and $\delta^{18}O$ measurements at 8,000, 15,000 (H1) and 20,000 (LGM) yr BP, respectively (Supplementary Table 1). For consistency, we re-calculated all age models in the same manner and transformed the proxy data into palaeotemperature estimates using the same set of calibrations (see Methods and Supplementary Information for details).

The transient behaviour of the proxy data across the deglaciation demonstrates that substantial and consistent changes in the thermal structure of the western Indian Ocean occurred during H1 and the YD. The two Mg/Ca–$\delta^{18}O$-derived temperature records indicate that SSTs were comparable to those of the LGM during the early part of H1, but then warmed slightly during the latest stage of the event (16–15 kyr BP) (Fig. 1a). After H1, there was an abrupt warming at 14.5 kyr BP associated with the Bølling/Allerød, then a cooling during the YD of about 0.5 °C (Fig. 1a). Similar to the Mg/Ca–$\delta^{18}O$ data, the $U^{K'}_{37}$-derived temperature records show, with the exception of site NIOP 905, cooling during early H1 followed by a slight warming before the end of the event at 14.5 kyr BP, and a small cooling (about 0.3 °C) during the YD (Fig. 1b).

To assess whether the observed trends in the Mg/Ca, $\delta^{18}O$ and $U^{K'}_{37}$ data agree with expected climatic responses during the deglaciation, we compare the proxy data to output from the TraCE-21ka (Simulation of Transient Climate Evolution over the past 21,000 yr) fully coupled climate model simulation,

[1]University of Arizona, Department of Geosciences, 1040 E 4th Street, Tucson, Arizona 85721, USA. [2]Woods Hole Oceanographic Institution, 266 Woods Hole Road, Woods Hole, Massachusetts 02543, USA. [3]Department of Meteorology and Bolin Centre for Climate Change Research, Stockholm University, Arrhenius Väg 16C, 106 91 Stockholm, Sweden. [4]Lamont-Doherty Earth Observatory of Columbia University, 61 Route 9W, Palisades, New York 10961, USA. *e-mail: jesst@email.arizona.edu

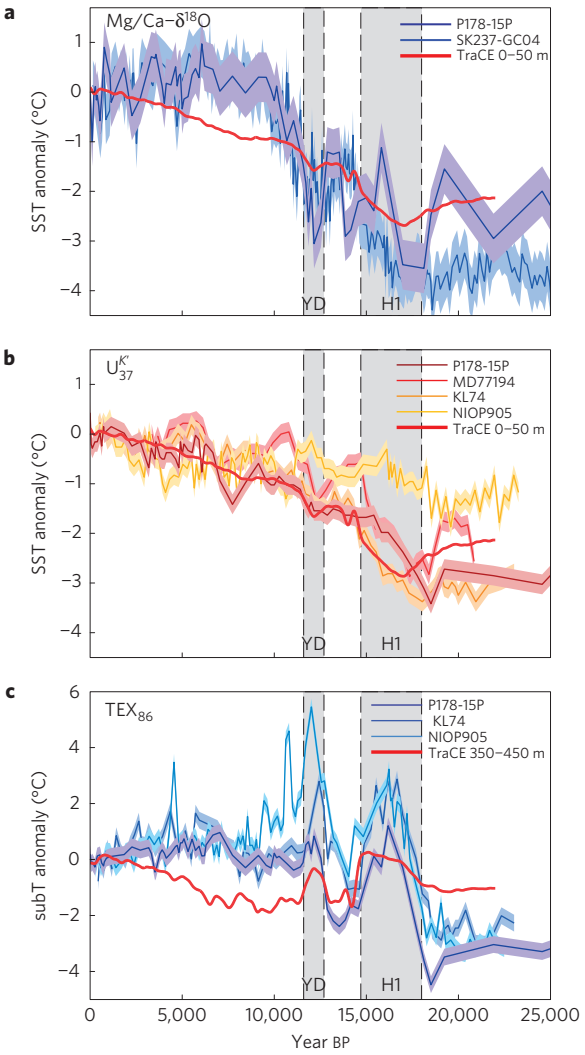

Figure 1 | The thermal evolution of the Arabian Sea across the last deglaciation, relative to the late Holocene (0–2,000 yr BP) mean. **a**, Mg/Ca–$\delta^{18}O$ sea surface temperature (SST), including data from P178-15P (this study) and SK237-GC04 (ref. 4). **b**, $U^{K'}_{37}$-based SST, including data from cores P178-15P (this study), MD77194 (ref. 6), KL74 (ref. 7) and NIOP905 (ref. 7). **c**, TEX_{86}-based subsurface temperatures (subT), including data from P178-15P (this study), KL74 (ref. 7) and NIOP905 (ref. 7). In each panel, the proxy data are overlain with simulated temperatures from the TraCE modelling experiment. The TraCE data are the average temperatures of the grid cells closest to the proxy sites represented in each panel. Shaded coloured areas represent 1σ analytical uncertainties.

a transient experiment conducted with the National Center for Atmospheric Research Community Climate System Model version 3 (NCAR CCSM 3.0) that includes orbital, greenhouse gas, ice sheet and freshwater forcing spanning 22 kyr BP to present[14]. We find remarkable agreement between the TraCE model results for the Arabian Sea region and the $U^{K'}_{37}$ data, with comparable LGM to Holocene annual mean temperature changes of about 2.5 °C, and surface coolings during H1 and the YD of 0.7 °C and 0.3 °C (Fig. 1b). Like both the $U^{K'}_{37}$ and the Mg/Ca–$\delta^{18}O$ data, the simulation indicates an early cooling during H1 followed by a gradual warming, and then an abrupt increase in temperature at the onset of the Bølling/Allerød (Fig. 1a,b). The Mg/Ca–$\delta^{18}O$ data differ from the TraCE simulation, and the $U^{K'}_{37}$ data, in that they show warm conditions during the early Holocene, relative to the late Holocene (Fig. 1a). Slight differences in the seasonal averaging of the foraminiferal and the alkenone signals may explain this inconsistency (see Supplementary Information).

In contrast to the Mg/Ca–$\delta^{18}O$ and $U^{K'}_{37}$ data, the TEX_{86} data indicate large and abrupt warmings during both H1 and the YD (Fig. 1c). Given the other proxy information, it is unlikely that these warm events represent a surface response. The organisms that produce GDGTs, pelagic Thaumarchaeota, may live throughout the upper water column, but, as nitrifiers, are more likely to inhabit the subsurface (50–200 m) than the surface layer[15]. In the Arabian Sea, intact polar GDGTs and thaumarchaeotal 16S rDNA copies peak near 170 m (ref. 16). It is likely, therefore, that TEX_{86} is recording subsurface thermal variability in the Arabian Sea. Generally speaking, subsurface temperatures co-vary with surface temperatures, allowing TEX_{86} to act as a SST proxy[17]. However, over longer geologic timescales, when the water column has probably seen substantial reorganization, surface and subsurface temperature variability can become decoupled. Accordingly, we use a subsurface calibration[18] to convert the TEX_{86} data to temperatures. TraCE data from 350 to 450 m water depth also show warming during H1 and the YD (Fig. 1c), corroborating the interpretation that TEX_{86} is recording a subsurface signal. However, the mean LGM to Holocene simulated temperature difference at the 350–450 m depth in TraCE is near zero (Fig. 1c). This suggests that the TEX_{86} signature of subsurface warming probably originates from a depth shallower than 350–450 m, and that the warming simulated by TraCE may not propagate far enough up the water column.

Taken together, the proxy time series data and the TraCE simulation indicate that the YD and H1 events are associated with surface cooling and subsurface warming—that is, a reduction in the upper-ocean temperature gradient. The thermal response to H1 in particular evolves through the span of the event, consisting of an early cooling followed by a gradual warming (Fig. 1). The gradual 'recovery' warming during the latter part of H1 is a regionally coherent feature of the TraCE simulation, but not evident in an idealized simulation of Heinrich Event 1 that includes only freshwater forcing (Supplementary Fig. 4). This difference suggests that the late H1 warming is primarily due to changes in orbital forcing and rising greenhouse gas levels associated with the deglaciation, and not the H1 event itself. To facilitate a direct comparison of the proxy information to the idealized H1 simulation that was originally used to determine that Indian Ocean SSTs were the driving component for monsoon failure[3], and diagnose the mechanisms that lead to the observed thermal response, we plot all available SST data spanning H1 (Supplementary Table 1) as the difference between the 15–17 kyr BP average and the mean deglacial climate state (that is, the LGM–H1 difference with the deglacial trend removed, see Methods; Fig. 2).

The SST proxy data indicate that there was regionally coherent cooling during H1 of $-0.9\,°C \pm 0.3$ (median value and 1σ standard error, Fig. 2a), and the TEX_{86} data indicate that this cooling was accompanied by a subsurface warming of $2.5\,°C \pm 0.2$ (Fig. 2b). These values are in excellent agreement with the simulated annual mean changes in SST and subsurface temperatures during H1 in the CCSM3 idealized H1 experiment, which show surface cooling between −0.5 and −1.5 °C over the Arabian Sea and warming ranging from 0.5 to 3 °C between 200 and 500 m depth (Fig. 3b and Supplementary Fig. 4). The surface cooling occurs very early in the simulation (Fig. 3c), whereas the subsurface warming develops during the peak of the event, and persists even as the surface cooling wanes (Fig. 3d).

This difference in timing between the surface and subsurface ocean reflects the separate, yet interconnected, mechanisms that drive each thermal shift. The nearly instantaneous cooling of the surface ocean suggests a response to atmospheric cooling associated with the hemispheric-wide reduction in temperatures as H1 begins. This cooling in turn drives a reduction in the monsoon strength and

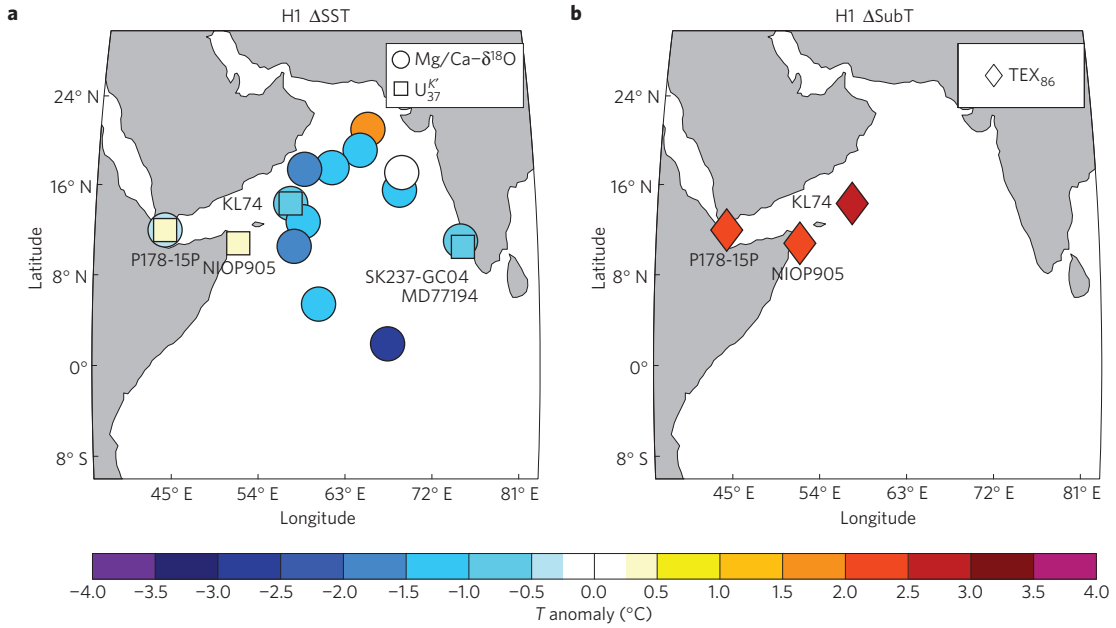

Figure 2 | Spatial expression of the surface and subsurface proxy response to the Heinrich 1 (H1) event, relative to mean deglacial conditions. a,**b**, Data are plotted as anomalies between 15–17 kyr BP (H1) and 19–21 kyr BP (LGM) with the deglacial warming trend removed (see Methods).

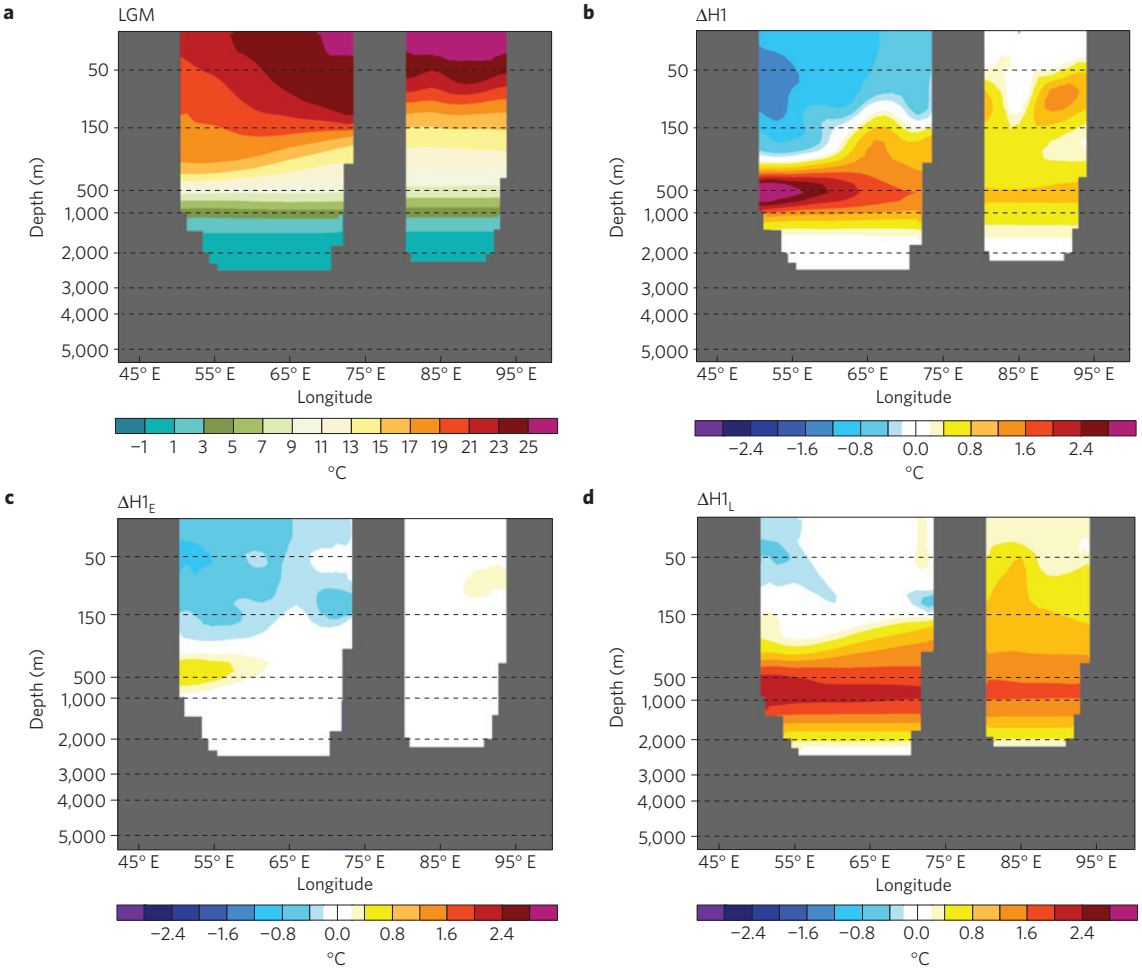

Figure 3 | Changes in the thermal structure of the Arabian Sea during an equilibrium simulation of an idealized Heinrich Event. a–**d**, Each panel shows a longitudinal transect at 15° N of the annual mean potential temperature (°C), including climatology for the LGM (**a**); changes during H1 (50–99 yr following the freshwater hosing) (**b**); changes during the earliest portion of the H1 event (1–20 yr following the freshwater hosing) (**c**); and changes during the latest portion of the H1 event (390–409 yr following the freshwater hosing) (**d**) relative to the LGM.

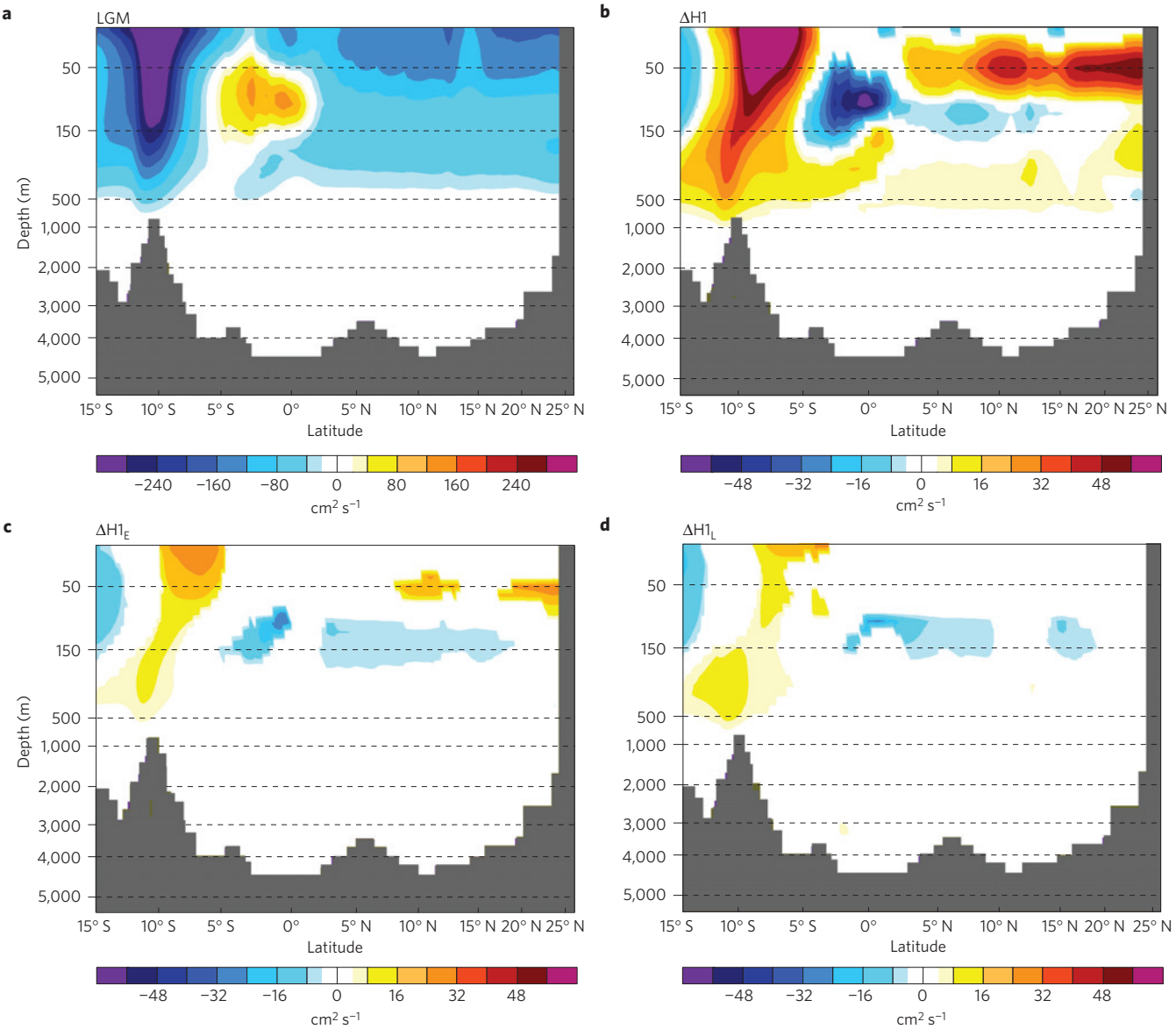

Figure 4 | Changes in ocean currents in the Arabian Sea in response to a simulated Heinrich Event. Each panel shows a latitudinal transect at 60° E of the annual mean stream function from the CCSM3 equilibrium simulation of H1, including climatology for the LGM (**a**); changes during H1 (**b**); changes during the earliest portion of the H1 event (**c**); and changes during the latest portion of the H1 event (**d**) relative to the LGM. Positive (negative) values indicate westward (eastward) movement of the ocean currents.

hence rainfall over the Indian subcontinent, as shown in detail by Pausata and colleagues[3]. The weaker monsoon winds then reduce the eastward movement of the upper-ocean currents, leading to reduced upwelling and the development of warmer subsurface temperatures during H1 and the YD (Fig. 4b). This dynamically induced warming is overwhelmed by atmospheric cooling at the surface, but dominates in the subsurface below about 300 m, with a maximum around 500 m water depth (Fig. 3b).

The Arabian Sea water column therefore underwent profound changes during the last deglaciation, with surface cooling, subsurface warming, and a corresponding reduction in the thermal stratification occurring in response to H1 and the YD. Regional records of total organic carbon[2], bulk nitrogen isotopic composition[19], biomarker ratios[20], and bromine concentrations[21] indicate reduced productivity and increased oxygenation during H1 and the YD, consistent with the destratification of the water column. Crucially, the proxy data analysed here confirm that the western Indian Ocean cooled during H1 and the YD, thereby providing the necessary mechanism to reduce the monsoon winds and cause dry conditions throughout the Afro-Asian monsoon domain. The fact that the cooling during H1 is relatively modest (about 0.5–1 °C) implies that the Indian monsoon system is very responsive to SST variability in the Indian Ocean, in agreement with model sensitivity studies[3,22]. The deglacial proxy data further emphasize that Arabian Sea SSTs are, in turn, sensitive to remote North Atlantic coolings, such that future prediction of Indian monsoon strength might consider the impact of weakening thermohaline circulation[23,24] in addition to enhanced warming in the Indian Ocean[25] and an increase, or changes, in aerosol emissions[26].

Methods

Methods and any associated references are available in the online version of the paper.

Received 8 July 2015; accepted 22 October 2015;
published online 7 December 2015

References

1. Overpeck, J., Anderson, D., Trumbore, S. & Prell, W. The southwest Indian Monsoon over the last 18,000 years. *Clim. Dynam.* **12,** 213–225 (1996).
2. Schulz, H., von Rad, U. & Erlenkeuser, H. Correlation between Arabian Sea and Greenland climate oscillations of the past 110,000 years. *Nature* **393,** 54–57 (1998).
3. Pausata, F. S. R., Battisti, D. S., Nisancioglu, K. H. & Bitz, C. M. Chinese stalagmite $\delta^{18}O$ controlled by changes in the Indian monsoon during a simulated Heinrich event. *Nature Geosci.* **4,** 474–480 (2011).
4. Saraswat, R., Lea, D. W., Nigam, R., Mackensen, A. & Naik, D. K. Deglaciation in the tropical Indian Ocean driven by interplay between the regional monsoon and global teleconnections. *Earth Planet. Sci. Lett.* **375,** 166–175 (2013).
5. Dahl, K. A. & Oppo, D. W. Sea surface temperature pattern reconstructions in the Arabian Sea. *Paleoceanography* **21,** PA1014 (2006).
6. Sonzogni, C., Bard, E. & Rostek, F. Tropical sea-surface temperatures during the last glacial period: A view based on alkenones in Indian Ocean sediments. *Q. Sci. Rev.* **17,** 1185–1201 (1998).
7. Huguet, C., Kim, J.-H., Sinninghe Damsté, J. S. & Schouten, S. Reconstruction of sea surface temperature variations in the Arabian Sea over the last 23 kyr using organic proxies (TEX_{86} and $U^{K'}_{37}$). *Paleoceanography* **21,** PA3003 (2006).
8. McManus, J. F., Francois, R., Gherardi, J.-M., Keigwin, L. D. & Brown-Leger, S. Collapse and rapid resumption of Atlantic meridional circulation linked to deglacial climate changes. *Nature* **428,** 834–837 (2004).
9. Vellinga, M. & Wood, R. A. Global climatic impacts of a collapse of the Atlantic thermohaline circulation. *Climatic Change* **54,** 251–267 (2002).
10. Hemming, S. R. Heinrich events: Massive late Pleistocene detritus layers of the North Atlantic and their global climate imprint. *Rev. Geophys.* **42,** RG1005 (2004).
11. Stager, J. C., Ryves, D. B., Chase, B. M. & Pausata, F. S. R. Catastrophic drought in the Afro-Asian monsoon region during Heinrich event 1. *Science* **331,** 1299–1302 (2011).
12. Tierney, J. E. & deMenocal, P. B. Abrupt shifts in horn of Africa hydroclimate since the last glacial maximum. *Science* **342,** 843–846 (2013).
13. Tierney, J. E., Ummenhofer, C. C. & deMenocal, P. B. Past and future rainfall in the Horn of Africa. *Sci. Adv.* **1,** e1500682 (2015).
14. Liu, Z. *et al.* Transient simulation of last deglaciation with a new mechanism for Bølling-Allerød warming. *Science* **325,** 310–314 (2009).
15. Karner, M., DeLong, E. & Karl, D. Archaeal dominance in the mesopelagic zone of the Pacific Ocean. *Nature* **409,** 507–510 (2001).
16. Schouten, S. *et al.* Intact polar and core glycerol dibiphytanyl glycerol tetraether lipids in the Arabian Sea oxygen minimum zone: I. Selective preservation and degradation in the water column and consequences for the TEX_{86}. *Geochim. Cosmochim. Acta* **98,** 228–243 (2012).
17. Tierney, J. E. & Tingley, M. P. A Bayesian, spatially-varying calibration model for the TEX_{86} proxy. *Geochim. Cosmochim. Acta* **127,** 83–106 (2014).
18. Tierney, J. E. & Tingley, M. P. A TEX_{86} surface sediment database and extended Bayesian calibration. *Sci. Data* **2,** 150029 (2015).
19. Altabet, M. A., Higginson, M. J. & Murray, D. W. The effect of millennial-scale changes in Arabian Sea denitrification on atmospheric CO_2. *Nature* **415,** 159–162 (2002).
20. Schulte, S., Rostek, F., Bard, E., Rullkötter, J. & Marchal, O. Variations of oxygen-minimum and primary productivity recorded in sediments of the Arabian Sea. *Earth Planet. Sci. Lett.* **173,** 205–221 (1999).
21. Caley, T. *et al.* Southern Hemisphere imprint for Indo-Asian summer monsoons during the last glacial period as revealed by Arabian Sea productivity records. *Biogeosci. Discuss.* **10,** 9315–9343 (2013).
22. Meehl, G. A. & Arblaster, J. M. Indian monsoon GCM sensitivity experiments testing tropospheric biennial oscillation transition conditions. *J. Clim.* **15,** 923–944 (2002).
23. Manabe, S. & Stouffer, R. J. Century-scale effects of increased atmospheric CO_2 on the ocean–atmosphere system. *Nature* **364,** 215–218 (1993).
24. Stocker, T. F. & Schmittner, A. Influence of CO_2 emission rates on the stability of the thermohaline circulation. *Nature* **388,** 862–865 (1997).
25. Du, Y. & Xie, S.-P. Role of atmospheric adjustments in the tropical Indian Ocean warming during the 20th century in climate models. *Geophys. Res. Lett.* **35,** L08712 (2008).
26. Meehl, G. A., Arblaster, J. M. & Collins, W. D. Effects of black carbon aerosols on the Indian monsoon. *J. Clim.* **21,** 2869–2882 (2008).

Acknowledgements

We thank F. He for assistance with the TraCE data. Funding for this research was provided by the National Science Foundation (Grant #OCE-1203892 to J.E.T.) and the International Meteorological Institute at Stockholm University, with contributions from the Center for Climate & Life at Lamont-Doherty Earth Observatory.

Author contributions

J.E.T. and F.S.R.P. designed the study. J.E.T. measured and analysed the TEX_{86} and $U^{K'}_{37}$ proxy data from the Gulf of Aden core, and synthesized previously published proxy data. P.deM. measured and analysed the $\delta^{18}O$ and Mg/Ca data from the Gulf of Aden core. F.S.R.P. designed and performed the model analysis and contributed to the interpretation of the proxy data. J.E.T. wrote the paper with contributions from all the authors.

Additional information

Supplementary information is available in the online version of the paper. Reprints and permissions information is available online at www.nature.com/reprints. Correspondence and requests for materials should be addressed to J.E.T.

Competing financial interests

The authors declare no competing financial interests.

Methods

Palaeoclimate proxy reconstructions. We compiled published, publicly archived data from the Arabian Sea that have sufficient chronology and time resolution to resolve the millennial-scale events of the last deglaciation, and also generated new $U^{K'}_{37}$, TEX_{86}, Mg/Ca and $\delta^{18}O$ data from Site P178-15P in the Gulf of Aden (see Supplementary Information for details). Supplementary Table 1 lists all of the data used in this study and their corresponding location and source references. To facilitate consistent inter-site comparison, we re-calibrated the age models of all sites, and calibrated proxy data to SSTs using the same set of calibrations. Specifically, we used the BAYSPAR subT calibration for TEX_{86} (ref. 18), the Indian Ocean calibration for $U^{K'}_{37}$ (ref. 27), and a new calibration, based on foraminiferal culture data, for jointly inferring SST from Mg/Ca and $\delta^{18}O$ (see Supplementary Information). As we are concerned only with anomalies, calibrated SSTs data are shown with their analytical uncertainties rather than the absolute calibration uncertainties (Fig. 1).

To calculate the anomaly associated with H1 against the background of deglacial warming (Fig. 2a,b) we applied a linear detrend to the time series data from 10 to 21 kyr BP and then calculated the H1 anomaly as the average difference between 15–17 kyr BP and 19–21 kyr BP. For the timeslice data, we calculated the H1 anomaly as the difference between the 15 kyr BP timeslice and the average of the 8 and 20 kyr BP timeslices.

Climate model simulations. To understand the transitory behaviour of western Indian Ocean climate and oceanography to the millennial-scale coolings of the last deglaciation, we analysed the TraCE-21ka simulation conducted with the NCAR CCSM3 coupled climate model[28]. The atmospheric model is the Community Atmospheric Model 3 (CAM3) with 3.75° × 3.75° horizontal resolution (T31) and 26 hybrid vertical levels. The ocean model is the NCAR implementation of the Parallel Ocean Program (POP) with 25 vertical levels. The longitudinal resolution of the ocean model is 3.6° and the latitudinal resolution is variable, with finer resolution near the equator (~0.9°). The model is coupled to a dynamic global vegetation module. The model is forced by realistic insolation, atmospheric CO_2, continental ice sheets and meltwater discharge, as described in detail in ref. 14.

To isolate the abrupt cooling during the H1 event from the 'background' warming induced by insolation and changing greenhouse gas forcing, we also analysed two equilibrium simulations: the reference case (LGM) and an idealized H1 experiment. The LGM experiment is a 440-yr integration of the National Center for Atmospheric Research CCSM3. The atmospheric model is the CAM3 with 2.8° × 2.8° horizontal resolution (T42) and 26 hybrid vertical levels. The experiment was forced by boundary conditions at the LGM, approximately 21,000 yr BP, including insolation, carbon dioxide concentration, the orography associated with the great ice sheets and a land configuration that reflects the lower LGM sea level[29]. The H1 experiment was performed by instantly adding 16 Sv-yr volume of freshwater to the upper 970 m of the North Atlantic and Arctic Oceans[30]. The initial conditions for this experiment were taken from year 400 in the LGM simulation. For the LGM climate, we use the average of the last 50 years of the LGM CCSM3 simulation; for the H1 climate, we analyse three time slices: the early period—H1E (the first 20 years following the water hosing); the period of maximum cooling—H1 (50–99 yr following the water hosing); and the latest period—H1L (390–409 yr following the water hosing).

Data. Data associated with this manuscript is publicly available at the NOAA NCDC: https://www.ncdc.noaa.gov/paleo/study/19420

Code Availability. All of the model data are publicly available at https://www.earthsystemgrid.org/home.htm

References

27. Sonzogni, C. *et al.* Temperature and salinity effects on alkenone ratios measured in surface sediments from the Indian Ocean. *Q. Res.* **47,** 344–355 (1997).
28. He, F. *Simulating Transient Climate Evolution of the Last Deglaciation with CCSM3* PhD thesis, Univ. Wisconsin-Madison (2010).
29. Otto-Bliesner, B. L. *et al.* Last glacial maximum and Holocene climate in CCSM3. *J. Clim.* **19,** 2526–2544 (2006).
30. Bitz, C., Chiang, J., Cheng, W. & Barsugli, J. Rates of thermohaline recovery from freshwater pulses in modern, last Glacial Maximum, and greenhouse warming climates. *Geophys. Res. Lett.* **34,** L07708 (2007).